Available online at www.sciencedirect.com
SCIENCE DIRECT®
Aerospace Science and Technology 8 (2004) 715–727
Aerospace Science and Technology
www.elsevier.com/locate/aescte

2D and 3D aerodynamic shape optimisation using the adjoint approach ☆

2D und 3D aerodynamischen Formoptimierung mittels Adjungiertenverfahren

J. Brezillon *, N.R. Gauger

DLR-Institute of Aerodynamics and Flow Technology, Lilienthalplatz 7, 38108 Braunschweig, Germany

Received 10 December 2003; received in revised form 28 June 2004; accepted 1 July 2004

Available online 11 September 2004

Abstract

The present paper aims at describing the potential of the adjoint technique for aerodynamic shape optimisation. After a brief description of the continuous adjoint formulation and the aerodynamic optimisation process developed at the DLR, specific requirements for an optimisation framework combined with the adjoint technique are introduced. The drag reduction at constant lift and pitching moment for the RAE2822 airfoil in transonic flow is then presented as validation case. An extension to multi-point optimisation demonstrates the capability of the framework to solve more complex problems. Finally, the wing-body optimisation of a supersonic commercial aircraft confirms the flexibility of the framework and the efficiency of the adjoint technique.

Zusammenfassung

In dem hier vorliegenden Artikel wird das Potential der Adjungiertenverfahren in der aerodynamischen Formoptimierung aufgezeigt. Zunächst wird eine kurze einführende Beschreibung so genannter kontinuierlicher adjungierter Formulierungen gegeben, die in der am DLR entwickelten Optimierungsumgebung Verwendung finden. Ferner werden die spezifischen Anforderungen an die verwendete Optimierungsschale für die Benutzung von Adjungiertenverfahren in der aerodynamischen Formoptimierung erläutert. Als Validierungsfall für dieses Optimierungsverfahren wird die Widerstandsreduktion des transsonischen RAE2822-Profils, unter den Nebenbedingungen eines konstanten Auftriebes und Nickmomentes sowie einer konstanten Profildicke, vorgestellt. Schließlich zeigt die Anwendung des Adjungiertenverfahrens für den Mehrpunktentwurf dieses Profils sowie der Flügel-Rumpf-Optimierung eines Überschallverkehrsflugzeuges, dass auch komplexere aerodynamische Optimierungsaufgaben mit diesem Verfahren in numerisch effizienter Weise gelöst werden können.

Keywords: Optimisation; Aerodynamic; Adjoint; Airfoil; Supersonic aircraft; Numerics

Schlüsselwörter: Optimierung; Aerodynamisch; Adjungiertenverfahren; Profil; Überschallverkehrsflugzeug; Numerische Verfahren

1. Introduction

Numerical simulation in aerodynamics is now mature enough to play an important role in design of new aircraft. A detailed aerodynamic shape optimisation can therefore be done with the help of accurate flow-solvers based on the Navier–Stokes, or at least the Euler equations. However, the prediction of the aerodynamic performance may still suffer from high computational costs on complex geometries and in combination with a design problem with large number of design variables, an efficient optimisation strategy has to be considered.

☆ This article was presented at the German Aerospace Congress 2003.

* Corresponding author.
E-mail address: joel.brezillon@dlr.de (J. Brezillon).

1270-9638/$ – see front matter
doi:10.1016/j.ast.2004.07.006

Search methods, such as genetic algorithms have been successfully applied in aerodynamic shape optimisation problems [27,28,32]. Such strategies are capable of finding a global optimum and are well-suited for problems with multiple objectives but at the cost of numerous flow evaluations, up to 5000 in some cases [27].

Gradient based methods are well known to be a more effective method and design improvements can be obtained in relatively few evaluations of the objective function and gradient. The gradient can be used directly to determine a search direction for the optimisation process or alternatively in conjunction with the objective function, 2nd order information of the goal function can be approximated. A full description of gradient based methods, starting from steepest descent, and proceeding to more effective strategies like quasi-Newton approaches can be found in [33]. Gradient based methods were first successfully applied to aerodynamic shape optimisation problems by Hicks et al. in 1974 [11]. It comes out that one of the main challenges for an effective gradient based method is an accurate and efficient computation of the gradient.

The finite differences approach is the most common way to compute the gradient and its implementation is straightforward: the gradient of the cost function with respect to the design variables is calculated by taking small steps in each and every design space. Unfortunately, the computational cost is prohibitive for large number of design variables and the accuracy is highly dependent of the step size. A way to overcome this accuracy problem consist of computing the finite differences gradient using complex variables [26]. This approach is highly accurate, insensitive to the step size but still dependent of the number of design variables. Furthermore the computation with complex variables requires even greater computational resources.

An improvement over finite differences methods consists of using the adjoint method and Pironneau [29] was the first to use it for design in fluid dynamics. Following this approach, the gradient is calculated by solving the adjoint equation. Once this equation has been solved, the cost of obtaining the required gradient is negligible. Consequently, the total cost of obtaining gradients is now independent of the number of design variables and depends only on the cost of one aerodynamic flow solution and one adjoint solution. This method has been applied to aeronautic design problems and can be subdivided into the continuous [12, 13,16,18,35] and the discrete approach [3,5,6]. For the continuous approach, the adjoint equation is derived from the continuous flow equations, and then discretised, while for the discrete approach, the adjoint equation is directly derived from the discrete flow equations. Anderson and Venkatakrishnan [1] analysed both the continuous and discrete adjoint methods for unstructured grids and implemented the discrete approach for viscous design problems. More recently, Nadarajah and Jameson [25,26] performed a comparison between continuous and discrete adjoints on structured meshes and they concluded that the discrete adjoint gradients have better agreement than the continuous ones with finite differences based on complex steps, but the difference is generally small. Furthermore, this difference decreases as the mesh size increases. In terms of the cost for derivation and implementation, the continuous adjoint is cheaper than the discrete adjoint and the structure of the aerodynamic solver can be relatively easily reused for solving the continuous adjoint problem. Such arguments are particularly attractive for development and maintenance of aerodynamic and adjoint codes.

At the DLR, dependable and efficient tools for aerodynamic simulation were developed and validated within the framework of the German aerospace research program, the MEGAFLOW CFD project [20]. In this context, the block-structured parallel Navier–Stokes solver FLOWer [19] has been developed and is intensively used by the DLR, aircraft industry and universities. For solving aerodynamic optimisation problems, the continuous adjoint approach is seen as promising, and within the MEGAFLOW II project [21,22], an adjoint solver has been developed accordingly. The starting point for this development was the acquisition of the Jameson code flo87s [13–15]. This code is a complete optimisation system which includes among other things an Euler as well as an adjoint Euler solver for structured single-block meshes. Instead of extending the flo87s code, as the original author did [17,30] to handle more complex applications, the DLR decided to implement an adjoint solver within the FLOWer code, following the same strategy as Jameson did. The philosophy was that after the implementation of the adjoint solver, all features of the FLOWer code are available for the adjoint mode (e.g. the capability to handle arbitrary multi-block topologies) [8,9].

The aim of the present paper is to describe the potential of the adjoint technique for aerodynamic shape optimisation. First, the theoretical background of the continuous adjoint approach is introduced and its implementation in FLOWer is validated on the transonic RAE2822 airfoil. The optimisation framework is then described and drag reduction at constant lift and pitching moment of the RAE2822 airfoil using the adjoint approach serves as validation case. The potential of the adjoint technique for aerodynamic shape optimisation is then demonstrated on two test cases, both defined within the European project AEROSHAPE [31]: the 2D multi-point drag optimisation under geometrical as well as physical constraints, and the wing body-optimisation of a supersonic commercial aircraft.

2. Continuous adjoint formulation

We first describe the principles of the so-called adjoint approach in general terms. Secondly, we present the continuous adjoint Euler equations and the adjoint formulations of the gradients of the cost functions for drag, lift and pitching moment. In this context ‘continuous’ means that the optimisation problem and its dual or adjoint formulation are

investigated on the level of the continuous control equations and cost functionals first, only later they are discretised.

2.1. Principles of adjoint formulations

Let $X = (X_i)_{i=1,\dots,n} \in \mathbb{R}^n$ denote the vector of design variables. Then X determines the shape geometry $C(X)$ and its physics $w(X)$, where $w \in \mathbb{R}^d$ is the vector of state variables. Furthermore, w is assumed to be the solution of the partial differential equations

$$R(X, w) = 0. \tag{1}$$

If the shape geometry is now perturbed from $C(X)$ to $C(X + \delta X)$, we get

$$R\big(X + \delta X, w(X + \delta X)\big) = 0. \tag{2}$$

Let now $I(X, w)$ denote the cost function of the optimisation problem. For a gradient based optimisation procedure, we have to determine the gradient

$$\nabla_X I = \frac{dI}{dX} = \frac{\partial I}{\partial X} + \frac{\partial I}{\partial w}\frac{\partial w}{\partial X} \tag{3}$$

of the cost function.

Using the brute force approach of finite differences, the gradient of the cost function can be estimated by using a first order forward-difference approximation

$$\nabla_X I = \left(\frac{I(X_i + \delta X_i) - I(X_i)}{\delta X_i} + \mathrm{O}(\delta X_i)\right)_{i=i,\dots,n}, \tag{4}$$

where the δX_i are the step sizes. This implies that one must solve Eqs. (1) once and Eqs. (2) n times.

Alternatively, one can expand (2) as a Taylor series at the point (X, w) and subtracting $R(X, w)$ on both sides. It ends up with

$$\delta R = \frac{\partial R}{\partial X}\delta X + \frac{\partial R}{\partial w}\delta w + \mathrm{O}\big(\|\delta X\|^2\big) = 0, \tag{5}$$

where

$$\delta w := \frac{\partial w}{\partial X}\delta X. \tag{6}$$

If we add now (5), multiplied by an arbitrary Lagrangian multiplier $\psi = (\psi_i)_{i=1,\dots,d} \in \mathbb{R}^d$ to Eq. (3), we get

$$(\nabla_X I)^{\mathrm{T}}\delta X = \frac{\partial I}{\partial X}\delta X + \frac{\partial I}{\partial w}\delta w + \psi^{\mathrm{T}}\left(\frac{\partial R}{\partial X}\delta X + \frac{\partial R}{\partial w}\delta w\right), \tag{7}$$

which is equivalent to

$$(\nabla_X I)^{\mathrm{T}}\delta X = \left(\frac{\partial I}{\partial X} + \psi^{\mathrm{T}}\frac{\partial R}{\partial X}\right)\delta X + \left(\frac{\partial I}{\partial w} + \psi^{\mathrm{T}}\frac{\partial R}{\partial w}\right)\delta w. \tag{8}$$

Now choose ψ such, that

$$\frac{\partial I}{\partial w} + \psi^{\mathrm{T}}\frac{\partial R}{\partial w} = 0 \tag{9}$$

holds: these are the adjoint equations to (1).

Finally we get

$$\nabla_X I = \frac{\partial I}{\partial X} + \psi^{\mathrm{T}}\frac{\partial R}{\partial X}. \tag{10}$$

In order to evaluate the adjoint gradient formulation (10), we have to solve Eqs. (1) just once and the adjoint equations (9) once and no other equation has to be solved. Now, we present the continuous adjoint Euler equations and the adjoint formulations of the gradients of the cost functions for drag, lift and pitching moment.

2.2. Continuous adjoint Euler equations

The continuous adjoint of the Euler equations is now introduced and the analysis is restricted to the 2D for reasons of convenience.

The steady Euler equations can be written as

$$\frac{\partial f}{\partial x} + \frac{\partial g}{\partial y} = 0 \text{ in } D, \tag{11}$$

where $\vec{n}^{\mathrm{T}}\vec{v} = 0$ on $C = C(X)$, with

$$w = \begin{pmatrix} \rho \\ \rho u \\ \rho v \\ \rho E \end{pmatrix}, \quad f(w) = \begin{pmatrix} \rho u \\ \rho u^2 + p \\ \rho uv \\ \rho uH \end{pmatrix},$$

$$g(w) = \begin{pmatrix} \rho v \\ \rho vu \\ \rho v^2 + p \\ \rho vH \end{pmatrix}, \quad \text{and} \quad \vec{n} = \begin{pmatrix} n_x \\ n_y \end{pmatrix}, \quad \vec{v} = \begin{pmatrix} u \\ v \end{pmatrix}.$$

On the farfield, free stream conditions are assumed. For a perfect gas

$$p = (\gamma - 1)\rho\left(E - \frac{1}{2}\vec{v}^2\right) \tag{12}$$

holds for the pressure, and finally C_p, C_D, C_L and C_m are defined as

$$C_p = \frac{2(p - p_\infty)}{\gamma M_\infty^2 p_\infty}, \tag{13}$$

$$C_D = \frac{1}{C_{\mathrm{ref}}}\int_C C_p(n_x\cos\alpha + n_y\sin\alpha)\,\mathrm{d}l, \tag{14}$$

$$C_L = \frac{1}{C_{\mathrm{ref}}}\int_C C_p(n_y\cos\alpha - n_x\sin\alpha)\,\mathrm{d}l, \tag{15}$$

$$C_m = \frac{1}{C_{\mathrm{ref}}^2}\int_C C_p\big(n_y(x - x_m) - n_x(y - y_m)\big)\,\mathrm{d}l. \tag{16}$$

The continuous adjoint Euler equations can be derived via the previous Lagrangian multiplier ansatz as

$$-\left(\frac{\partial f}{\partial w}\right)^{\mathrm{T}}\frac{\partial \psi}{\partial x} - \left(\frac{\partial g}{\partial w}\right)^{\mathrm{T}}\frac{\partial \psi}{\partial y} = 0 \quad \text{in } D, \quad \text{where} \tag{17}$$

$$n_x\psi_2 + n_y\psi_3 = -d(I) \quad \text{on } C(X) \tag{18}$$

on the wall and

$$\delta x_\xi, \dots, \delta y_\eta = 0, \quad \delta w = 0 \quad \text{on } B(X) \tag{19}$$

on the farfield. (ξ, η) are the grid points in body fitted coordinates.

The right hand side $d(I)$ of the wall boundary condition of the adjoint Euler equations is dependent on the cost function I, and is given below, for the drag, lift and pitching moment respectively:

$$d(C_D) = \frac{2}{\gamma M_\infty^2 p_\infty C_{\text{ref}}}(n_x \cos\alpha + n_y \sin\alpha), \tag{20}$$

$$d(C_L) = \frac{2}{\gamma M_\infty^2 p_\infty C_{\text{ref}}}(n_y \cos\alpha - n_x \sin\alpha), \tag{21}$$

$$d(C_m) = \frac{2}{\gamma M_\infty^2 p_\infty C_{\text{ref}}^2}\big(n_y(x - x_m) - n_x(y - y_m)\big). \tag{22}$$

The adjoint farfield boundary condition describes just that the geometrical position of the farfield is fixed and free stream conditions apply there. For more details on the derivation and the theoretical background of the adjoint Euler equations see [8].

2.3. Gradient formulation

The components of the gradient $\nabla_X I = (\delta_i I)_{i=1,\dots,n}$ can be determined via an integration only over the adjoint solution and the metric sensitivities $\delta x_\xi \dots \delta y_\eta$ and

$$\delta I = -\int_C p(-\psi_2 \delta y_\xi + \psi_3 \delta x_\xi)\,\mathrm{d}l + K(I) - \int_D \psi_\xi^{\mathrm{T}}(\delta y_\eta f - \delta x_\eta g) + \psi_\eta^{\mathrm{T}}(-\delta y_\xi f + \delta x_\xi g)\,\mathrm{d}A \tag{23}$$

is obtained, where $K(I)$ is a term dependent on the cost function I.

For the gradient of the drag, $K(I)$ is

$$K(C_D) = \frac{1}{C_{\text{ref}}}\int_C C_p(\delta n_x \cos\alpha + \delta n_y \sin\alpha)\,\mathrm{d}l, \tag{24}$$

for the gradient of the lift

$$K(C_L) = \frac{1}{C_{\text{ref}}}\int_C C_p(\delta n_y \cos\alpha - \delta n_x \sin\alpha)\,\mathrm{d}l, \tag{25}$$

is used, and for the gradient of the pitching moment

$$K(C_m) = \frac{1}{C_{\text{ref}}^2}\int_C C_p \delta\big(n_y(x - x_m) - n_x(y - y_m)\big)\,\mathrm{d}l, \tag{26}$$

is used.

The main advantages of the adjoint approach can now be evidenced: after evaluating the aerodynamic and the corresponding adjoint states, each component of the gradient is directly obtained by evaluating the integral (23) which only requires the variation of the metrics. We are now independent of the number of design variables, in the sense that no further flow computations are required to evaluate the gradient.

This way of computing the gradient was implemented for two dimensional problems, and is used for airfoil optimisations presented in this paper. However, its extension to 3D cases was not easy, most particularly due to the metric sensitivities, $\delta x_\xi \dots \delta y_\eta$ in Eq. (23). Indeed, these terms have to be evaluated not only at the body surface but in the complete field, and if one thinks of complex 3D multi-block meshes, these terms may be difficult to obtain. Therefore, it was decided to use another formulation for computing the gradient.

2.4. Gradient formulation using surface integral

During the AEROSHAPE project, P. Weinerfelt suggested to us a gradient formulation that he developed together with Enoksson [35] that only requires an integration over the body. This formulation is based on integral properties and an explanation of the derivation is outside the scope of this paper. The interested reader can have a look in the above reference.

Here, only the gradient for the drag is indicated:

$$\delta(C_D) = \int_C \nabla\big(\varphi - (w^H \psi)\vec{v}\big)\delta\vec{n}\,\mathrm{d}\vec{S} \tag{27}$$

with B the surface of the solid body,

$$w^H = \begin{pmatrix} \rho \\ \rho\vec{v} \\ \rho H \end{pmatrix}, \quad \text{and} \quad \varphi = \begin{pmatrix} Cp\cos\alpha \\ Cp\sin\alpha \\ 0 \end{pmatrix}.$$

This formulation was implemented and is used to solve the 3D optimisation case presented at the end of the paper.

3. Validation of the adjoint approach

The test case for the validation of the adjoint Euler solver FLOWer and the method of computing the gradient is the inviscid transonic RAE2822 airfoil. The flight conditions are $M_\infty = 0.73$ and $\alpha = 2^\circ$ as Mach number and angle of attack respectively.

The first step in validating the adjoint based design method is to compare the gradients of the drag, lift and pitching moment it produces with the approximated gradients obtained by finite differences. One of the problems of such comparisons comes from the way to compute the gradients with finite differences, more precisely the well-known problem of choosing the adequate finite step, named δX_i in Eq. (4). A small step size is desired to reduce the truncation errors $O(\delta X_i)$. On the other hand, a too small change of geometry would produce a too small change of aerodynamic loads which could be of the same order of magnitude as the numerical noise: the resulting approximated gradient would not be exact at all. Plotting the approximated gradient according to the step size indicates a specific range lying between the two mentioned boundaries where the gradient remains almost independent to the step size. Therefore, it is possible to approximate the gradient with finite differences,

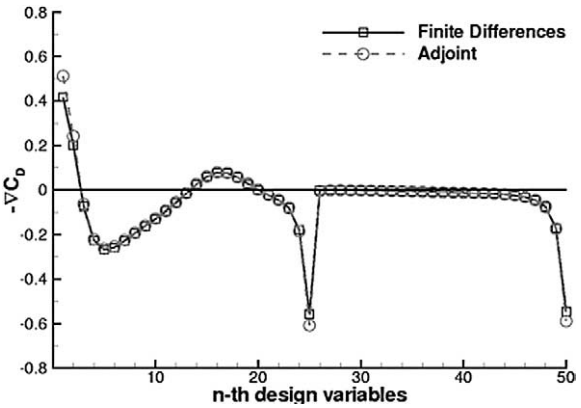

Fig. 1. Gradient of the drag for the RAE2822 airfoil (50 B-spline parameters – $M_\infty = 0.73$, $\alpha = 2°$).

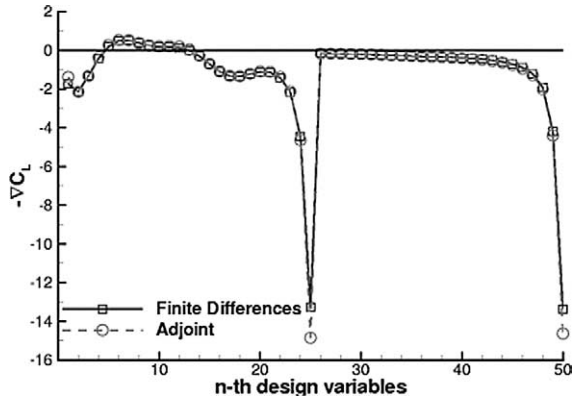

Fig. 2. Gradient of the lift for the RAE2822 airfoil (50 B-spline parameters – $M_\infty = 0.73$, $\alpha = 2°$).

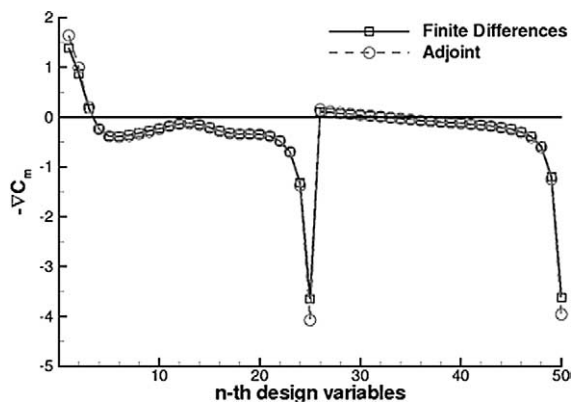

Fig. 3. Gradient of the pitching moment for the RAE2822 airfoil (50 B-spline parameters – $M_\infty = 0.73$, $\alpha = 2°$).

but this requires not only $n + 1$ evaluations, but $m \times n + 1$ evaluations, with m the number of different steps size tried. In order to facilitate the comparison with the adjoint approach, we consider now that the gradient is evaluated with only one step size in every design direction (i.e. that m is set to 1).

The design variables are 50 control points of a B-spline parameterisation. The finite differences gradients are provided by forward differencing and thus 51 Euler solutions are required to get the complete gradients. In order to avoid numerical noise in the evaluation of the aerodynamic coefficients, a convergence of 10 orders of magnitude in RMS density residuals is required for each computation.

For the adjoint approach just one Euler and three Euler adjoint solutions are necessary. The Euler field provides not only the aerodynamic state at the surface, but it is also used to evaluate the Jacobi matrix in the whole field for computing the adjoint equations (17). Therefore a well converged Euler field is required, and the same convergence as for finite differences is used. In counterpart, it was observed that a comparably low level of convergence for the adjoint solution is sufficient to accurately compute the gradient. A decrease of 4 orders of magnitude in RMS residual of the first adjoint component is applied because further convergence has a negligible effect on the gradient. These observations corroborate well with the conclusion of Jameson et al. [26].

Figs. 1–3 show the components of the gradients of the drag, lift, and pitching moment, respectively, according to the design variables. The 50 design variables span from the leading edge to the trailing edge along first the upper side and then the lower side. All three figures show a very good conformity of the finite differences and adjoint gradients.

Via adjoint approach, each component of the gradient is obtained after the evaluation of the integral (23) which requires in addition to the adjoint field, the mesh sensitivity. Because both adjoint and aerodynamic solvers have the same efficiency and fewer iterations are needed for the adjoint solution, the total time needed for the evaluation of the gradient is roughly equivalent to the time needed to deeply converge the main solution: to evaluate the 3 gradients, the adjoint approach requires the equivalent time of 4 aerodynamic computations which is 13 times less than with finite differences.

4. The optimisation framework

Next to code development, an optimisation framework was also under investigation during the MEGAFLOW project and the optimisation system MEPO has been accordingly developed by the DLR in co-operation with the Technical University of Braunschweig and Airbus Bremen. This system proved its efficiency in solving aerodynamic problems [2], but the structure was not flexible enough to be able to easily integrate new modules. Thus a collaboration with the Synaps Ingenieur-Gesellschaft mbH was initiated in order to assess the capabilities of the SynapsPointer® Pro optimisation framework [7] to integrate modules that were to be developed within the MEGAFLOW II project, especially the adjoint approach.

4.1. Requirements for aerodynamic optimisation

Modularity and flexibility of an aerodynamic optimisation framework is of main interest. Indeed, for aerodynamic

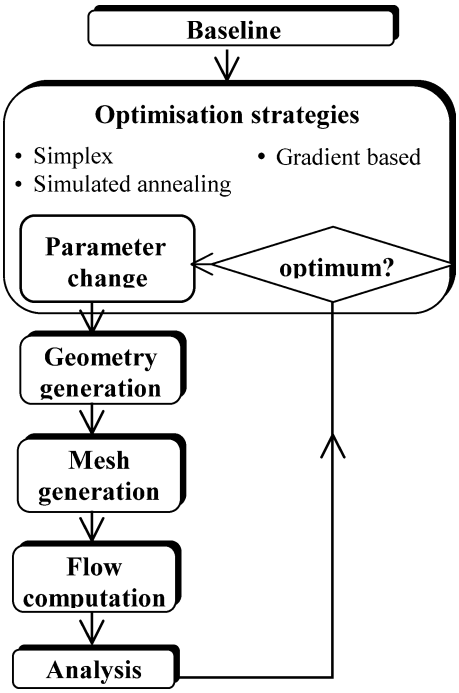

Fig. 4. Structure of the aerodynamic optimisation loop.

shape optimisation, the framework should connect all elementary modules necessary to associate a given geometry to an aerodynamic state, and to carry this information over to the optimiser. A general aerodynamic optimisation loop showing the main building blocks is presented in Fig. 4.

The SynapsPointer® Pro optimisation framework has been retained as optimisation framework because it allows an easy construction of the aerodynamic chain and manages the connection to different optimisers. Furthermore, this framework automatically runs processes in parallel and therefore allows a decrease of the turn around time.

The framework is open enough to allow also the integration of user-supplied optimisers and accordingly the strategies of constrained steepest descent and that of the commercial DOT tool from Vanderplaats [34] were successfully integrated and used for solving cases presented in this paper.

4.2. Specific requirements for the adjoint technique

Let us now consider an unconstrained problem. With a gradient-based strategy, the approach for solving such a problem consists first in determining the optimal search direction in the design space, that leads to the most promising decrease of the cost function, and then in finding a local minimum along this optimal search direction. These two steps are repeated until no more reduction of the cost function can be achieved.

The optimiser typically manages the evaluation of the optimal direction by finite differences. This means evaluations of the variation of the cost function in each direction of the design space. In an n-dimensional design space, all variations are obtained after $n + 1$ evaluations of the flow. The evaluation of a single cost function can take a lot of time and, in the frame of a detailed aerodynamic optimisation, this brute force strategy is particularly costly when the number of design variables is large. Furthermore this approach does not guarantee the accuracy of the gradient, as discussed in Section 3.

As mentioned earlier, efficiency and accuracy can be improved by defining and solving an adjoint problem. In this case the cost of evaluating the optimal direction is now independent of the number of design variables. Using this attractive technique now requires providing the optimiser not only with the cost function but also with the optimal direction, which is a vector of dimension n. This new functionality has been implemented in the framework and was used for solving all applications presented below.

5. Airfoil optimisation

5.1. Test case definition

The optimisation problem of drag reduction at constant lift, pitching moment and fixed angle of attack is chosen for the validation of the optimisation process. The aerodynamic coefficients are evaluated in inviscid flow and the test case conditions are the same as for the validation of the continuous adjoint approach: the starting geometry is the RAE2822 airfoil, the Mach number and angle of attack are set to respectively $M_\infty = 0.73$ and $\alpha = 2^\circ$. Before showing the results, the aerodynamic chain is described and the way in which aerodynamic constraints have been handled is presented.

5.2. Description of the aerodynamic chain

For the parameterisation the airfoil is decomposed into thickness and camber distributions, but only the camberline is modified. This procedure allows the thickness of the airfoil to remain unchanged during the optimisation process.

Results first obtained with a B-spline parameterisation were not smooth and satisfying enough. Therefore the parameterisation was switched to the basis of Hicks–Henne functions [10], which are "sine bumps" in form. Twenty Hicks–Henne functions have been assigned to the camberline.

Throughout the optimisation process, meshes for the modified geometries were generated by the DLR tool MegaCads [4]. In the present case, all meshes are of the same topology (a C-mesh topology around the airfoil) and of the same size (321×57).

The flow solution is computed using the FLOWer code in Euler mode. Therefore the drag improvement consists only of the wave drag decrease. The flow solution is sufficiently converged with typically 10 orders of magnitude of RMS residuals which is easily obtained by means of the multigrid option available in FLOWer. This level of convergence

ensures a minimum of noise in the evaluation of the cost function which is of crucial importance for gradient based optimisation. For the adjoint computation, only 4 orders of magnitude are enough to get accurate gradients.

5.3. Treatment of the aerodynamic constraints

At this point, it is assumed that gradients of the drag, lift and pitching moment are accurately determined with the adjoint approach.

As mentioned in the previous part, for optimisation problems without constraints, the optimal direction along which a local minimum is searched corresponds to the direction of the gradient of the cost function. However, for constrained problems, this optimal direction can lead to a violation of the constraints. One way to solve constrained problems consists then in finding a "feasible" direction along which the cost function decreases while constraints are kept constant. In other words, along this "feasible" direction, the constraints should have no variation. As an example, let us consider a single constraint termed Q depending on its position in the n-dimensional design space. It is mathematically well known that the variation of Q along a particular direction in the design space can be approximated, at first order accuracy, by the scalar product of the gradient of Q with the vector pointing in the specified direction. Therefore, a direction normal to the gradient of Q yields a null scalar product and no deviation of Q, at least in a neighbourhood where first order accuracy is predominant. Furthermore, finding such a direction orthogonal to the gradient has more than one solution and defines in fact an hyperplane of dimension $n-1$: any vector included in the subspace orthogonal to the gradient of Q is a candidate for no-variation of Q.

Decreasing the drag while maintaining constant lift can be done by projecting the drag-gradient onto the hyperplane normal to the lift-gradient. This approach, called in this paper "the constrained steepest descent", is simple to implement and can be generalised to several constraints using a Schmidt orthogonalisation. The resulting direction leads to a decrease of the cost function, while keeping the constraints constant, at least if the variation is small enough not to introduce second order effects.

In conclusion, the treatment of the constraints can be based on an optimal direction that depends not only on the gradient of the cost function, but also on the gradients of the constraints themselves.

5.4. Results

Fig. 5 shows the evolution of the drag, lift and pitching moment over the optimisation steps. An optimisation step consists of evaluation of the aerodynamic state, the necessary gradients and the line search for finding a better minimum. For the present case, 9 evaluations of gradients and

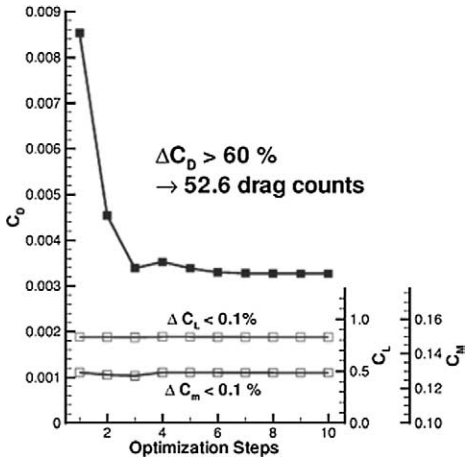

Fig. 5. Evolution of the aerodynamic coefficients for drag reduction at fixed lift, pitching moment and angle of attack of the RAE2822 airfoil ($M_\infty = 0.73$, $\alpha = 2°$).

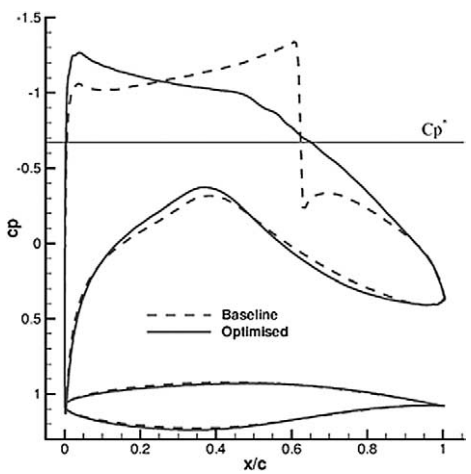

Fig. 6. Initial and final pressure distribution ($M_\infty = 0.73$, $\alpha = 2°$).

40 evaluations of the aerodynamic coefficients were necessary to converge the optimisation problem. Compared to the classical finite differences approach, the present optimisation would be more than 3 times faster.

Upon convergence, a decrease of more than 60% of the cost function (drag) is achieved while both the constraints (lift and pitching moment) remain unchanged. As expected, the strong shock appearing on the RAE2822 airfoil is eliminated at the end of the design process as shown in Fig. 6. The pressure distribution is also characterised by an increase of the suction peak and an increase of the rear loading in order to keep the lift constant. An analysis of the optimal geometry evidences a lower camber in the front part and a higher one in the rear part.

Due to the magnitude of the changes in the cost function at the beginning of the optimisation problem and to the nonlinearity of this problem, small deviations in the constraints do occur. Therefore the pitching moment and the lift are corrected at the fourth step to retrieve the initial value and this correction introduces an increase of the cost function as can

be seen in Fig. 5. The optimisation procedure is then continued until convergence. It is interesting to point out that close to the optimal solution, the optimisation process converges linearly, as for steepest descent approach: this confirms that the continuous adjoint provides an accurate gradient, also near convergence, and no accuracy problems occur.

This first result is meant as a validation of the complete optimisation strategy: from the parameterisation of the geometry down to the handling of constraints with the continuous adjoint.

6. Multi-point optimisation

6.1. Test case definition

The design problem is now the minimisation of a linear combination of the drag at three flow conditions for the RAE2822 airfoil under aerodynamic and geometric constraints. This case was one of several exercises defined within the European research programme AEROSHAPE. The objective function reads:

$$Obj = \sum_{i=1}^{3} W_i C_D(\alpha_i, M_i), \tag{28}$$

where C_D is the drag coefficient as a function of the angle of incidence α and the Mach number M, and W_i are the weighting coefficients.

The three aerodynamic design conditions read as follow:

- $\alpha_1 = 2.8°$, $M_1 = 0.734$, $Re_1 = 6.5 \times 10^6$, $W_1 = 2$,
- $\alpha_2 = 2.8°$, $M_2 = 0.754$, $Re_2 = 6.2 \times 10^6$, $W_2 = 1$,
- $\alpha_3 = 1.8°$, $M_3 = 0.680$, $Re_3 = 5.7 \times 10^6$, $W_3 = 1$.

The aerodynamic constraints on each design point are:

- the angle of attack is fixed,
- the lift is not allowed to decrease,
- only a variation of $\pm 2\%$ on the pitching moment is allowed.

Four additional geometrical constraints are set:

- the maximum thickness is frozen
- the thickness at 5% chord should not be less than 96% of the initial one,
- the leading edge radius should be equal to or greater than 90% of the initial leading edge radius,
- the trailing edge angle should not be less than 80% of that of the initial geometry.

6.2. Optimisation strategy

In order to broader the design space and then allow the optimiser to find a better shape fulfilling all aerodynamic constraints, the parameterisation was improved by allowing changes of both the camberline and thickness of the RAE2822 geometry. One can notice that all geometrical constraints are applied on the thickness of the airfoil, and the camberline has no constraints. Therefore, Hicks–Henne bump functions are used for deforming the camberline. For the thickness law, a B-spline parameterisation was preferred because it allows handling the geometrical constraints. The use of the adjoint approach allows one to have a cost independent of the number of design variables for the computation of the gradients. In total, 29 design variables have been chosen, 9 for the thickness distribution and 20 for the camberline distribution.

In the same way as for the validation case, the structured mesh is provided by the MegaCads grid generator.

As for the aerodynamic flow, the Reynolds-averaged Navier–Stokes equations are solved using FLOWer. Turbulence effects are taken into account with the cost-effective algebraic Balwin–Lomax model rather than with a more accurate two-equation transport model. The required gradients are approximated by using the inviscid adjoint approach and such approach could be called an "hybrid optimisation strategy". It is important to point out that the resulting gradients take only into account the inviscid effects which for airfoil drag optimisation leads to only decrease the wave drag. For the RAE2822, a shock does occur at the first and the second aerodynamic design point. On the other hand such an airfoil produces no wave drag at the third design point and so no improvement is expected at this condition: the third design point is seen as additional constraints to the optimisation problem, established to avoid alteration of performance at subsonic conditions.

The evaluation of a single goal function and the associated gradient requires 3 aerodynamic and 3 adjoint computations each time. To decrease the turn around time, these evaluations are performed in parallel on 3 nodes of a Linux cluster, each processor treating independently an aerodynamic design condition.

The use of the "constrained steepest descent" approach, described in the previous section, failed to treat this multi-constraint problem. Indeed, if this strategy allows finding the direction to maintain the constraints constant, a specific treatment has to be developed when a constraint is violated, like the correction step introduced at the fourth step in the previous optimisation. In the present multi-point case, the "constrained steepest descent" allowed decreasing the drag but some constraints were so violated that it was impossible to find a correction step that simultaneously fulfilled all constraints. Thus, we decided to use a more advanced optimisation strategy which can handle complex multi-constrained problems. Vanderplaats proposed in [33] various ways to handle the constraints, starting from the simple strategy of the penalty function method to the more advanced "Sequential Quadratic Programming" (also called SQP). The main drawback of strategies based on penalties is to find the proper weight to penalise the objective function when a constraint is violated. This problem does not arise on strategies using gradient information, like the "method of feasible di-

rection" or the "SQP" method [33]. Both methods are available in the DOT package and were tried to solve the current multi-point problem. The best results, exhibited in the next section, were obtained with the "method of feasible direction". This strategy is more effective than the "constrained steepest descent" because it now computes how deep the constraints are violated (if they are violated) and accordingly computes the optimal direction to reduce the objective and at the same time retrieve the violated constraints. The correction step is now directly integrated into the optimal direction.

6.3. Results

The complete optimisation took less than 1 day on a Linux cluster and required 5 optimisation steps, which represent 55 evaluations of the goal function (i.e. 55×3 aerodynamic computations), 5×3 adjoint computations for the gradient of the objective function and 22 adjoint computations for the constraints. The minimum was found at the 4th step, after 40×3 aerodynamic computations. In the 5th step, no better optimum was found and the optimisation process stopped. It is important to point out that the adjoint solver computes gradients based on inviscid computations. Therefore, these gradients have to be seen as an approximation of the exact gradients and the optimiser faced problems finding a better minimum. This problem will vanish using viscous adjoint approach, as planned in future.

At the end of the optimisation process, the two first design points show a decrease of 23 and 32 drag counts respectively, whereas the drag for the third design point increases slightly by about 1 drag count. All geometric and aerodynamic constraints are fulfilled and Table 1 summarises the aerodynamic performances.

Compared to the original geometry, the optimised shape is characterised by a change of the thickness distribution, with a decrease in the front part and an increase in the rear part (Fig. 7). The maximum thickness location is slightly shifted toward the trailing edge. The camber is slightly increased in the rear part.

The pressure distributions plotted on Fig. 8 presents a reduction of the shock strength, which can be particularly seen on the main design point. An increase of the suction peak can be seen for all 3 design points.

Table 1
2D multi-point aerodynamic optimisation

	Design pt 1	Design pt 2	Design pt 3
W	2	1	1
α (°)	2.8	2.8	1.8
M_∞	0.734	0.754	0.680
$C_D{}^{b} \times 10^{-4}$	209.6	301.6	116.7
ΔC_D (%)	−10.9	−10.8	+1.00
ΔC_L (%)	+1.5	+1.5	0.0
ΔC_m (%)	−1.98	−1.99	+1.63

[b] Refers to the baseline geometry.

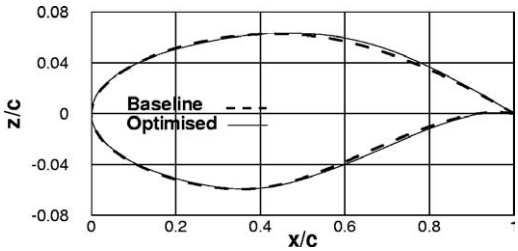

Fig. 7. Baseline and optimised geometries for the multi-point drag optimisation.

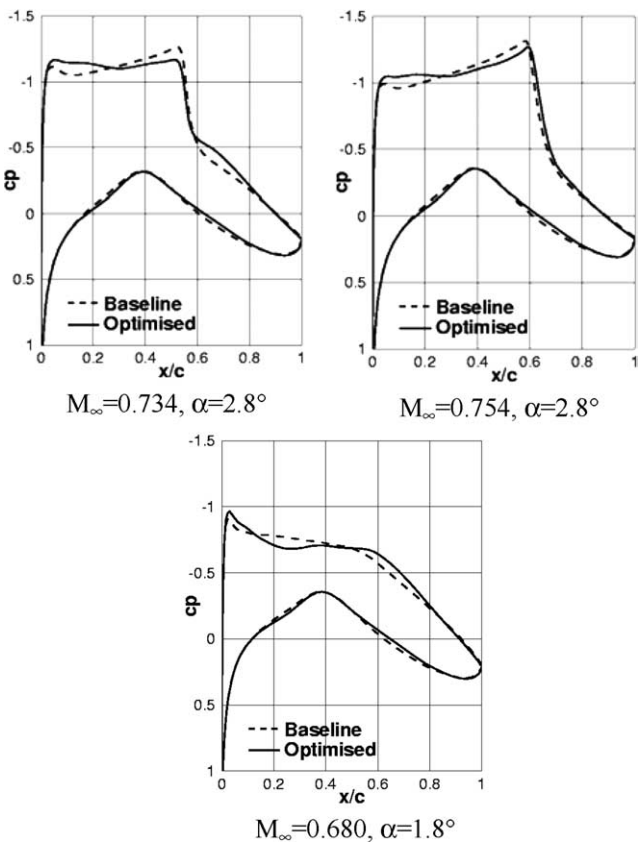

Fig. 8. Pressure distribution obtained for the multi-point drag optimisation.

7. Optimisation of a supersonic commercial aircraft

7.1. Test case definition

One of the AEROSHAPE test cases is the optimisation of a supersonic transport wing/body configuration. The baseline geometry is based on the EUROSUP geometry [23,24], which is a supersonic commercial aircraft of 252 seats capacity, designed for 5500 nautical miles range with a supersonic cruise flight at Mach number $M_\infty = 2.0$. In the framework of the EUROSUP research programme a number of geometry modifications were introduced in order to ease CFD grid generation and analysis work and this simplified geometry is the datum geometry for the AEROSHAPE exercise (Fig. 9).

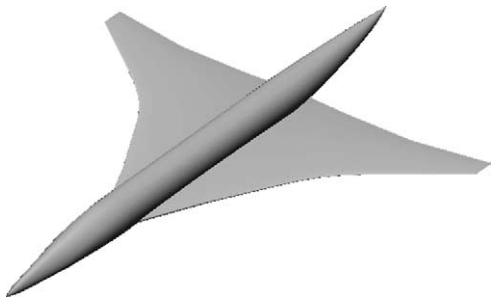

Fig. 9. Geometry of the Supersonic Transport Aircraft.

Two design test cases were defined within the European project AEROSHAPE and in this paper only the most interesting exercise, called the demonstration exercise, is presented.

The aim of the exercise is to demonstrate the capability of the optimisation method to handle many design parameters with acceptable costs. The optimisation goal is to minimise the drag at a fixed lift coefficient of $C_L = 0.12$. The fuselage incidence is allowed to change in order to maintain the lift coefficient but it should not be greater than 4 degrees to the onset flow.

The design variables have to parameterise the wing as well as the fuselage. A minimum allowable value of the fuselage radius and a minimum wing thickness law were imposed in order to prevent unrealistic aircraft.

7.2. Parameterisation

In order to use the full potential of the adjoint technique, no specific restrictions are set to define the parameterisation and 84 design parameters are used as follows.

The wing is parameterised with 74 design variables, which allow changing the twist, the thickness and the camberline at specific wing sections:

- the thickness deformation is based on B-splines curves in order to freely set the maximum thickness, the chordwise position of the maximum thickness, the leading edge radius and the trailing edge angle at 8 wing sections. The positions of the sections are chosen with respect to the spanwise distribution of the geometrical constraints on maximum thickness,
- the camber line is modified at 8 wing sections by adding Hicks–Henne bump functions to the initial geometry,
- the twist distribution is described by a Bezier curve defined with 10 nodes.

After geometrical modifications of each wing section, the geometry of the resulting wing is constructed by linear lofting.

The fuselage contraction is parameterised with 10 design variables, which change the radial distribution of the body in the streamwise direction. After deformation, the cross section became of elliptical form. The body centreline is kept unchanged during the optimisation. The intersection of wing and fuselage is recalculated automatically by MegaCads for each new configuration.

7.3. Mesh generation

The mesh generation is performed by MegaCads running in batch mode and based on a script file: for each new geometry, a new mesh with the same topology is created. The grid is of a structured mono-block type with about 230,000 cells. This mesh has been designed to have 3 multigrid levels.

7.4. Aerodynamic and gradient computations

At Mach 2, the main aerodynamic effects are well predicted using the Euler equations. Therefore, the aerodynamic states are computed by FLOWer running in Euler mode. The baseline method employs a central space discretisation with artificial viscosity and convergence is accelerated using local time stepping, implicit residual smoothing and multigrid techniques.

The constraint on the lift is handled using the target lift mode available in FLOWer which automatically adjusts the angle of attack to reach the desired lift. In such case, Jameson et al. propose to compute the associated gradient by only a single adjoint computation [30]: the adjoint now predicts the variation of the drag associated to a change of the shape and the angle of attack necessary for maintaining the lift constant. Such adjoint formulation has been implemented in FLOWer and is used to solve the present problem. The gradient is computed with the help of the surface formulation described in Section 2.4.

The pitching moment is only monitored during the optimisation and no constraint is applied on it.

All the computations are done on the DLR's high-performance supercomputer, the NEC-SX5.

7.5. Optimisation strategy

In the present optimisation problem, the unique aerodynamic constraint is the lift, which is handled directly by FLOWer and the geometrical constraints are automatically fulfilled during the parameterisation. Therefore, the optimiser deals with an unconstrained problem and unconstrained strategies like the "Variable Metric Methods" based on Broydon–Fletcher–Goldfarb–Shanno (BFGS) algorithm available in DOT and a quasi-newton trust region were tried. For the present test case, the method based on the BFGS algorithm was the most efficient and all results presented below were achieved using this method.

7.6. Results

Fig. 10 shows the evolution of the drag coefficient during the optimisation. About 8 optimisation steps were required

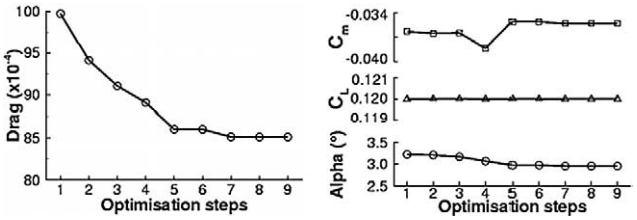

Fig. 10. Evolution of the SCT performances during the optimisation.

Table 2
Performance improvement for the SCT case

	α (°)	$C_D \times 10^{-4}$	C_L	C_m	C_L/C_D
Baseline	3.23	99.7	0.12	0.0363	12.03
Optimum	2.96	85.1	0.12	0.0353	14.10

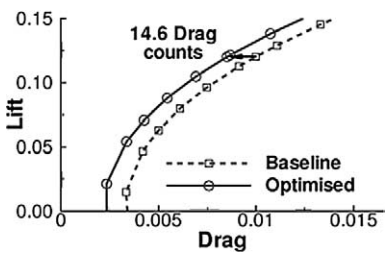

Fig. 11. Polar for the baseline and optimised geometries (M = 2.0).

to achieve the optimum, which represents about 54 aerodynamic computations and 8 adjoint flow evaluations: this approach would be more than 11 times faster than using brute force optimisation based on finite differences. The optimum configuration has 14.6 less drag counts than the baseline. It can be seen on the right of Fig. 10 that FLOWer keeps the lift constant during the complete optimisation and the angle of attack decreases slightly by about 0.3 degrees. The pitching moment, which is just monitored, increases by about 2.8%. Table 2 summarises the aerodynamic performances for the baseline and the optimum geometries.

At this point, it is interesting to analyse the evolution of the performance around the design point. Fig. 11 shows the polar both for the baseline and the improved geometries. It can clearly be seen that there is an almost constant reduction of the drag for the optimised geometry, not only located at the main design point ($C_L = 0.12$) but over the entire polar.

The body radius law in the streamwise direction is presented in Fig. 12: while body sections located close to the wing apex are expanded, with a maximum at $x = 30$ m, sections close to the wing trailing edge are contracted up to the minimum allowed radius. Such deformation is not surprising if one looks at the evolution of the area rule [36] along the streamwise direction as represented in Fig. 13. One can see in Fig. 14 the maximum wing thickness distribution in spanwise direction. At the end of the optimisation, the maximum thickness satisfies the constraints.

The geometry of the wing is plotted at 3 different spanwise sections – left-hand side of Figs. 15, 16 and 17. One can clearly see two different types of airfoil:

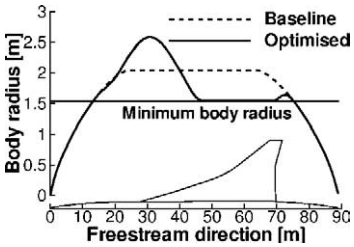

Fig. 12. Radius for the baseline and optimised geometries.

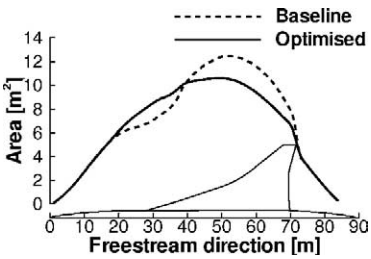

Fig. 13. Area rule for the baseline and optimised geometries.

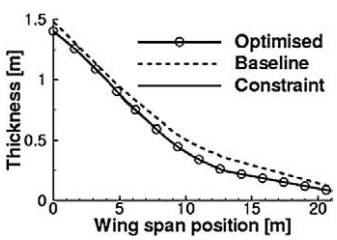

Fig. 14. Thickness law for the baseline and optimised geometries.

- for the first half wing sections close to the root, airfoils are mainly characterised by a round leading edge, with a shift of the maximum thickness location to the leading edge,
- for sections located close to the wing tip, the radius of the leading edge become smaller and the maximum thickness locations are shifted to the trailing edge.

One can see only a slight modification of the wing twist but it can be noticed that the wing sections plotted do not take into account the change of angle of incidence: the optimised wing has in fact a decrease of the inflow, coming from the change of angle of incidence (α varies from 3.23° to 2.96°) and this can be also seen as a constant twist modification. A deformation of the twist is in fact not independent of the angle of incidence and it seems that during the optimisation process, the angle of incidence has the bigger influence.

The pressure distributions are also plotted for the 3 corresponding wing sections – right-hand side of Figs. 15–17. The pressure peak is reduced all over the wing and lift gain should be obtained for sections located between the root and the crank. This is confirmed by a load analysis of the wing which shows an almost constant decrease of the drag over the complete wing with a lift increase for sections mainly located between $\eta = 0.3$ and $\eta = 0.6$.

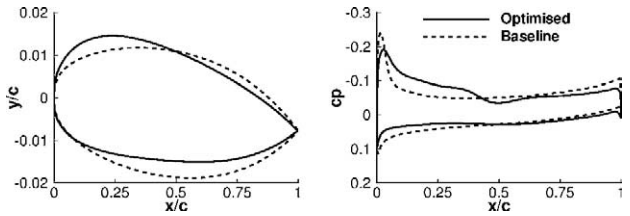

Fig. 15. Wing section and pressure distribution at $\eta = 0.24$.

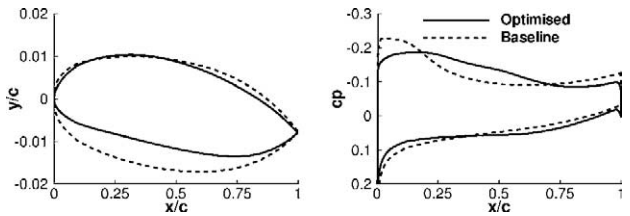

Fig. 16. Wing section and pressure distribution at $\eta = 0.49$.

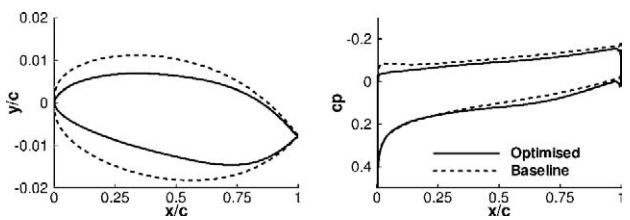

Fig. 17. Wing section and pressure distribution at $\eta = 0.92$.

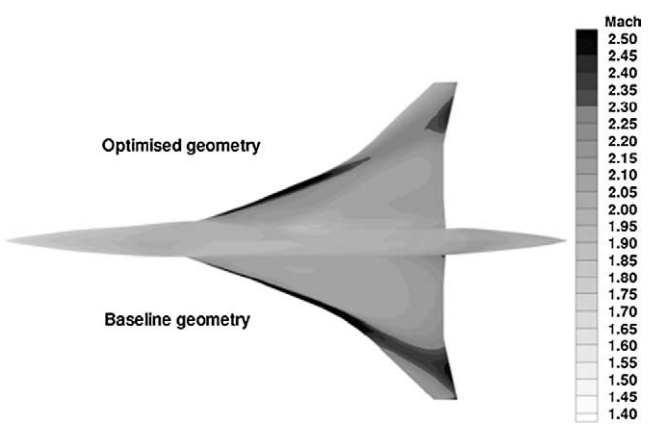

Fig. 18. Mach number distribution over the baseline and optimised geometries.

Fig. 18 gives a 3D Mach number distribution over the baseline and designed aircraft. The effect of the optimisation is particularly noticeable on the wing apex where lower velocities occur compared to the baseline geometry.

8. Conclusion and outlook

A new optimisation framework has been tested and its superiority in terms of flexibility has been demonstrated. This framework was successfully coupled with the adjoint technique and a step forward in terms of efficiency has been achieved. This system has first been validated for the drag reduction at constant lift and pitching moment for the RAE2822 airfoil in inviscid transonic flow. The resulting geometry is a shock free airfoil fulfilling all constraints. The extension of this configuration to a multi-point optimisation confirms the capability of the framework to treat more complex problems. The efficiency of the adjoint approach has also been demonstrated on the wing-body optimisation of a supersonic transport aircraft in inviscid flow where a lot of CPU time has been saved compared to brute force approaches. These results confirm that the combination of the SynapsPointer® Pro framework with the adjoint approach allows faster aerodynamic shape optimisations, making them attractive in an industrial context.

The extension to the use of the adjoint approach based on the Navier–Stokes equations allows the treatment of more complex applications, like those encountered in high lift cases. The development of the viscous adjoint solver has started and promising results have already been achieved during the European project AEROSHAPE. The same development – a viscous continuous adjoint – is also planed for the unstructured TAU code allowing a step forward in terms of efficiency and flexibility for complex configurations.

References

[1] W.K. Anderson, V. Venkatakrishnan, Aerodynamic design optimization on unstructured grids with a continuous adjoint formulation, AIAA 97-0643, 35th Aerospace Sciences Meeting and Exhibit, Reno, Nevada, January 1997.

[2] J.K. Axmann, M. Hadenfeld, O. Frommann, Parallel numerical airplane wing design, in: New Results in Numerical and Experimental Fluid Mechanics: Contributions to the 10th AG STAB/DGLR Symposium, Vieweg Verlag, 1996.

[3] F. Beux, A. Dervieux, Exact-gradient shape optimization of a 2D Euler flow, Finite Elements in Analysis and Design 12 (1992) 281–302.

[4] O. Brodersen, M. Hepperle, A. Ronzheimer, C.C. Rossow, B. Schoening, The parametric grid generation system MegaCads, in: Numerical Grid Generation in Computational Field Simulations; Proceedings of the 5th International Conference, Mississippi State Univ., Mississippi, 1996, pp. 353–362.

[5] G.W. Burgreen, O. Baysal, Three-dimensional aerodynamic shape optimization of wings using discrete sensitivity analysis, AIAA J. 34 (9) (1996) 1761–1770.

[6] J. Elliott, J. Peraire, Aerodynamic design using unstructured meshes, AIAA 96-1941, 1996.

[7] O. Frommann, SynapsPointerPro V2.50, Synaps Ingenieur-Gesellschaft mbH, Bremen, Germany, 2002.

[8] N.R. Gauger, Das Adjungiertenverfahren in der aerodynamischen Formoptimierung, DLR-Report No. DLR-FB-2003-05, ISSN 1434-8454, 2003.

[9] N.R. Gauger, J. Brezillon, Aerodynamic shape optimization using adjoint method, J. Aero. Soc. India 54 (3) (2002) 247–254.

[10] R.M. Hicks, P.A. Henne, Wing design by numerical optimization, J. Aircraft 15 (1978) 407–412.

[11] R.M. Hicks, E.M. Murman, G.N. Vanderplaats, An assessment of airfoil design by numerical optimization, NASA TM X-3092, Ames Research Center, California, July 1974.

[12] A. Iollo, M. Salas, S. Ta'asan, Shape optimization governed by the Euler equations using an adjoint method, ICASE report 93-78, November 1993.

[13] A. Jameson, Aerodynamic design via control theory, J. Scientific Comput. 3 (1988) 233–260.
[14] A. Jameson, Computational aerodynamics for aircraft design, Science 245 (1989) 361–371.
[15] A. Jameson, Optimum aerodynamic design via boundary control, AGARD-R-803, 1994, pp. 3.1–3.33.
[16] A. Jameson, Optimum aerodynamic design using CFD and control theory, AIAA 95-1729, in: AIAA 12th Computational Fluid Dynamics Conference, San Diego, 1995.
[17] A. Jameson, L. Martinelli, N.A. Pierce, Optimum aerodynamic design using the Navier–Stokes equations, Theoret. Comput. Fluid Dynamics 10 (1998) 213–237.
[18] A. Jameson, N.A. Pierce, L. Martinelli, Optimum aerodynamic design using the Navier–Stokes equations, AIAA 97-0101, AIAA 35th Aerospace Sciences Meeting and Exhibit, Reno, 1997.
[19] N. Kroll, B. Eisfeld, H.M. Bleecke, FLOWer, in: Notes on Numerical Fluid Mechanics, vol. 71, Vieweg Verlag, Braunschweig, 1999, pp. 58–68.
[20] N. Kroll, C.C Rossow, K. Becker, F. Thiele, MEGAFLOW – a numerical flow simulation system, in: 21st ICAS Symposium, Melbourne, Australia, 1998, paper 98-2.7.4.
[21] N. Kroll, C.C. Rossow, K. Becker, F. Thiele, The MEGAFLOW project, Aerosp. Sci. Technol. 4 (2000) 223–237.
[22] N. Kroll, C.C. Rossow, D. Schwamborn, K. Becker, G. Heller, MEGAFLOW – a numerical flow simulation tool for transport aircraft design, in: ICAS 2002 Congress, 2002, paper 1.10.5.
[23] D.A. Lovell, Aerodynamic research to support a second generation supersonic transport aircraft – the EUROSUP project, Eccomas 98 (1998).
[24] D.A. Lovell, European research of wave and lift dependent drag for supersonic transport aircraft, AIAA Paper No. 99-3100, 1999.
[25] S. Nadarajah, A. Jameson, A comparison of the continuous and discrete adjoint approach to automatic aerodynamic optimization, AIAA 38th Aerospace Sciences Meeting and Exhibit, AIAA-2000-0667, Reno, NV, January 2000.
[26] S. Nadarajah, A. Jameson, Studies of the continuous and discrete adjoint approaches to viscous automatic aerodynamic shape optimization, AIAA 2001-2530, 2001.
[27] B. Naujoks, L. Willmes, H. Werner, T. Back, M. Schutz, Multi-point airfoil optimization using evolution strategies, in: Proceedings of ECCOMAS, Barcelona, Spain, 2000.
[28] J. Periaux, M. Sefrioui, B. Stoufflet, B. Mantel, E. Laporte, Robust genetic algorithms for optimization problems in aerodynamic design, in: Genetic Algorithms in Engineering and Computer Sciences, Wiley, New York, 1995.
[29] O. Pironneau, On optimum design in fluid mechanics, J. Fluid Mech. 64 (1974) 97–110.
[30] J. Reuther, A. Jameson, J. Farmer, L. Martinelli, D. Saunders, Aerodynamic shape optimization of complex aircraft configurations via an adjoint formulation, AIAA 96-0094, Reno, 1996.
[31] V. Selmin, Multi-point aerodynamic shape optimization: the AEROSHAPE project, in: Proceedings of ECCOMAS, Barcelona, Spain, 2000.
[32] D. Tse, Y. Chan, Multi-point design of airfoils by genetic algorithm, in: 8th Annual Conference of the CFD Society of Canada, Montreal, Canada, 2000.
[33] G.N. Vanderplaats, Numerical Optimization Techniques for Engineering Design, McGraw-Hill Series in Mechanical Engineering, ISBN 0-07-066964-3, 1984.
[34] G.N. Vanderplaats, DOT Users Manual – Ver. 5.0, Vanderplaats Research & Development, Colorado Springs, 2001.
[35] P. Weinerfelt, O. Enoksson, Numerical methods for aerodynamic optimization, in: 8th International Symposium on Comp. Fluid Dynamics, Bremen, Germany, 1999.
[36] R.T. Whitcomb, J.R. Sevier, A supersonic area rule and an application to the design of a wing-body combination with high lift-drag ratios, NASA TR R-72, 1960.